CityU
香港城市大學
City University of Hong Kong
專業 創新 胸懷全球
Professional·Creative
For The World

CityU Scholars

Iridium(III) Blue Phosphors with Heteroleptic Carbene Cyclometalates Isomerization, Emission Tuning, and OLED Fabrications

Wu, Yixin; Huang, Manli; Cheng, Lin; Zhang, Junyao; Pan, Yi; Yiu, Shek-Man; Lau, Kai Chung; Yan, Jie; Yang, Chuluo; Chi, Yun

Published in:
Angewandte Chemie - International Edition

Published: 10/03/2025

Document Version:
Final Published version, also known as Publisher's PDF, Publisher's Final version or Version of Record

License:
CC BY

Publication record in CityU Scholars:
Go to record

Published version (DOI):
10.1002/anie.202421664

Publication details:
Wu, Y., Huang, M., Cheng, L., Zhang, J., Pan, Y., Yiu, S.-M., Lau, K. C., Yan, J., Yang, C., & Chi, Y. (2025). Iridium(III) Blue Phosphors with Heteroleptic Carbene Cyclometalates: Isomerization, Emission Tuning, and OLED Fabrications. *Angewandte Chemie - International Edition*, *64*(11), Article e202421664. https://doi.org/10.1002/anie.202421664

Citing this paper
Please note that where the full-text provided on CityU Scholars is the Post-print version (also known as Accepted Author Manuscript, Peer-reviewed or Author Final version), it may differ from the Final Published version. When citing, ensure that you check and use the publisher's definitive version for pagination and other details.

General rights
Copyright for the publications made accessible via the CityU Scholars portal is retained by the author(s) and/or other copyright owners and it is a condition of accessing these publications that users recognise and abide by the legal requirements associated with these rights. Users may not further distribute the material or use it for any profit-making activity or commercial gain.

Publisher permission
Permission for previously published items are in accordance with publisher's copyright policies sourced from the SHERPA RoMEO database. Links to full text versions (either Published or Post-print) are only available if corresponding publishers allow open access.

Take down policy
Contact lbscholars@cityu.edu.hk if you believe that this document breaches copyright and provide us with details. We will remove access to the work immediately and investigate your claim.

Download date: 20/04/2025

Check for updates

How to cite: *Angew. Chem. Int. Ed.* **2025**, *64*, e202421664
doi.org/10.1002/anie.202421664

VIP **Blue OLEDs** *Very Important Paper*

Iridium(III) Blue Phosphors with Heteroleptic Carbene Cyclometalates: Isomerization, Emission Tuning, and OLED Fabrications

Yixin Wu[+], Manli Huang[+], Lin Cheng[+], Junyao Zhang, Yi Pan, Shek-Man Yiu, Kai Chung Lau, Jie Yan,* Chuluo Yang,* and Yun Chi**

Abstract: Ir(III) complexes are particularly noted for their excellent photophysical properties in giving blue OLED phosphors. In this study, two distinctive carbene pro-chelates LAH_2^+ and LBH_2^+ (or LCH_2^+) were employed in preparation of heteroleptic Ir(III) complexes, to which LAH_2^+ bears a cyano substituted benzoimidazolium along with N-mesityl appendage, while LBH_2^+ (or LCH_2^+) carries the symmetrical benzoimidazolium entity. Notably, the reversible equilibration at high temperature was observed for ***m***,***f*-ct14** and ***m***,***f*-ct15** with a single LA chelate. In contrast, only the *mer*-substituted ***m*-ct16** was obtained upon employing two LA chelates. All Ir(III) complexes exhibited blue photoluminescence ($\Phi_{PL} \geq 78\,\%$) with short radiative lifetimes ($\tau_{rad} \leq 1.05\,\mu s$) in solution. The Ph OLED device with ***m*-ct16** afforded an external quantum efficiency (EQE) of 22.8 % at 5000 $cd \cdot m^{-2}$. Moreover, the hyper-OLED based on ***m*-ct16** and v-DABNA exhibited EQE_{1000} of 32.1 % (EQE recorded at 1000 $cd \cdot m^{-2}$) and J_{90} of 15.0 $mA\,cm^{-2}$ (current density at 90 % of max. EQE). Its suppressed efficiency roll-off (EQE of 32.1 % and 27.7 % at 1000 $cd \cdot m^{-2}$ and 10000 $cd \cdot m^{-2}$) demonstrated a milestone in fabrication of blue OLED devices.

Introduction

Organic light-emitting diodes (OLEDs) have been widely utilized in manufacturing the optoelectronic products such as displays, monitors, and lighting luminaries.[1] These devices were composed of multi-layered architectures, including electrodes, carrier transporting materials, hosts and emitters; the last are responsible for giving luminescence with three elemental colours, i.e., red, green and blue.[2] Due to the lowered emission energy of red and green emitters, plenty of them were available in actual commercial applications. Particularly, the emergence of transition-metal phosphors that can utilize all electrically generated excitons (both the singlet and triplet) provides a breakthrough to the red and green emitting OLEDs,[3] leaving blue emitters as one of the remaining research challenges in both the academic and industrial sectors.[4]

As to the blue emitters, both phosphors and thermally activated delayed fluorescence (TADF) materials have attracted the uttermost attention in recent years. Their common advantage is the theoretical unitary internal quantum efficiency (IQE) due to the effective harvesting of all generated excitons during operation. However, TADF emitters suffered from the intrinsic long triplet lifetime and slow exciton recycling,[5] giving severe efficiency roll-off at the higher current density. Therefore, heavy main group atom (s) such as sulphur and selenium were incorporated into the pure organic TADF molecules to resolve such deficiency.[6] Despite the initial success, the inferior carbon-chalcogen bond strength may lead to premature decomposition and unsatisfactory device longevity. Hence, the transition-metal based blue phosphors, particularly those with central Ir(III) and Pt(II) metal atoms, may still be the promising OLED emitters.[7] In fact, tetradentate Pt(II) emitters have been actively investigated as the probable candidates for their better stabilized multi-dentate chelating interaction and narrowband phosphorescence.[8] Concurrently, Ir(III) emitters bearing solely the dual N-aryl substituted carbene cyclometalates could be the alternative blue OLED emitters for their promising stability and efficiency induced by a total of six strengthened Ir–C coordinative interactions, and shortened radiative lifetime of approx. one microsecond.[9] However, as to these Ir(III) carbene emitters, only the facially (*fac*) substituted counter-

[*] Y. Wu,[+] L. Cheng,[+] J. Zhang, Y. Pan, S.-M. Yiu, K. Chung Lau, J. Yan, Y. Chi
Department of Chemistry, Department of Materials Science and Engineering, Center of Super-Diamond and Advanced Films (COSDAF), City University of Hong Kong, Hong Kong SAR,,
E-mail: kaichung@cityu.edu.hk
jyanae@connect.ust.hk
yunchi@cityu.edu.hk
M. Huang,[+] C. Yang
Shenzhen Key Laboratory of New Information Display and Storage Materials, College of Materials Science and Engineering, Shenzhen University, Shenzhen, 518055 P. R. China,
E-mail: clyang@szu.edu.cn
[+] Y.W., M.H. and L.C. contributed equally to this work

© 2025 The Author(s). Angewandte Chemie International Edition published by Wiley-VCH GmbH. This is an open access article under the terms of the Creative Commons Attribution License, which permits use, distribution and reproduction in any medium, provided the original work is properly cited.

 © 2025 The Author(s). Angewandte Chemie International Edition published by Wiley-VCH GmbH

parts are obtained till now, while those with meridional (*mer*) structures are essentially lacking.[10]

In the present investigation, we design and synthesize two distinctive classes of carbene chelates, LAH_2^+ and LBH_2^+ (or LCH_2^+), whose structural drawings are depicted in Scheme 1. First, both carbene chelates possess dual N-aryl substituents; therefore, unlike their N-alkyl analogues, there will be no uncoordinated N-alkyl appendage upon formation of Ir(III) carbene complexes, giving improved physical stability and, probably, better performances for the as-fabricated OLEDs. In addition, there is an electron-withdrawing cyano group on the benzoimidazolium fragment of LAH_2^+ for lowered ligand-centred energy gap, such that the blue emission can be expected upon formation of the Ir(III) emitters.[11] Thirdly, the N-mesityl group of LAH_2^+ and the symmetrical nature of both LBH_2^+ and LCH_2^+ imposed a profound restriction to the chelating mode, greatly reducing the expected products, particularly to those with the *mer*-configuration. Hence, the selection of these two chelates led to the syntheses of Ir(III) complexes with greatly simplified coordination configurations (i.e., both *mer*- and *fac*-forms) as shown in Scheme 2. Our results not only break the myth that the carbene cyclometalates with bulky N-mesityl substituent can never give stable Ir(III) complex, but also reveal a clear relationship of coordination isomerism vs. designs of carbene cyclometalates. Furthermore, their fundamentals and potentials in serving as OLED phosphors are addressed in the forthcoming session.

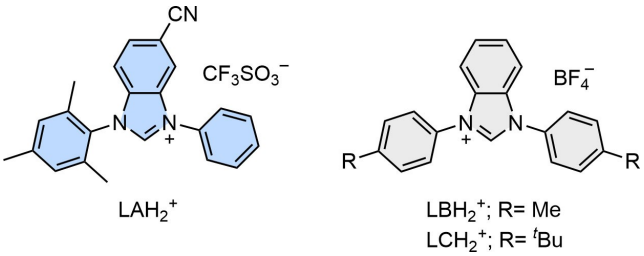

Scheme 1. Structural drawings of the employed carbene pro-chelates LAH_2^+, and LBH_2^+ and LCH_2^+.

Results and Discussion

Syntheses of Pro-Chelate and Ir(III) Complexes

The asymmetrical benzo[d] imidazol-3-ium pro-chelate LAH_2^+ bearing both the cyano substituent and N-mesityl appendage was prepared using the synthetic protocols shown in Scheme S1 of Supporting Information. Firstly, the 4-bromo-3-nitrobenzonitrile was converted to 4-(mesitylamino)-3-nitrobenzonitrile using Pd-catalyzed Buchwald–Hartwig coupling. Next, the 1-mesityl-1H-benzo[d] imidazole-5-carbonitrile was prepared by iron catalyzed reduction of 4-(mesitylamino)-3-nitrobenzonitrile in presence of formic acid, followed by in situ cyclization. Finally, catalytic quaternization with bis (phenyl) iodonium triflate in the presence of cuprous oxide gave the desired pro-chelate LAH_2^+ in high yield.[12] Alternatively, the symmetrical benzo [d] imidazol-3-ium pro-chelates LBH_2^+ and LCH_2^+ were obtained following the literature precedent,[13] c.f., Scheme S2.

Preparation of the heteroleptic Ir(III) complexes was next executed using $[Ir(COD)(\mu\text{-}Cl)]_2$ as the metal source reagent. Synthesis of Ir(III) complexes ***m***, ***f*-ct14**, as well as their *tert*-butyl counterparts ***m***, ***f*-ct15**, involved heating of four equiv. of LBH_2^+ (or LCH_2^+) with $[Ir(COD)(\mu\text{-}Cl)]_2$ in refluxing acetonitrile, giving the speculative diiridium intermediate $[Ir(LB)_2(\mu\text{-}Cl)]_2$ or $[Ir(LC)_2(\mu\text{-}Cl)]_2$, respectively.[14] After then, the reaction mixture was evacuated to dryness and the residue was immediately treated with two equiv. of the carbene pro-chelate LAH_2^+ in refluxing *o*-dichlorobenzene (180 °C). This operation afforded a mixture of *mer*- and *fac*-substituted Ir(III) complexes ***m***, ***f*-ct14** and ***m***, ***f*-ct15** in an approx. ratio of 3:4 and 1:7, respectively. Equilibration between *mer*- and *fac*-isomers was also possible upon raising the temperature to 214 °C in 1,2,4-trichlorobenzene and in the presence of sodium acetate and *p*-toluene sulfonic acid. The isomeric ratios at equilibration are akin to their synthetic yields reported earlier. This behaviour confirmed the distinctive influence of methyl and *t*-butyl substituent of N-aryl groups, and high stability and facile isomerism among these Ir(III) complexes.

Next, we varied the stoichiometric ratio of carbene pro-chelates LBH_2^+ vs LAH_2^+, with an attempt to probe the influence of carbene cyclometalates. Hence, we lowered the

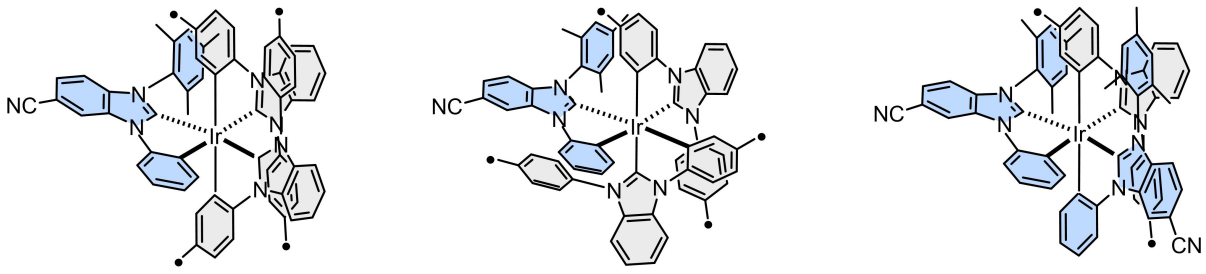

m-ct14, • = Me
m-ct15, • = ^{t}Bu

f-ct14, • = Me
f-ct15, • = ^{t}Bu

m-ct16, • = Me

Scheme 2. Structural drawings of the studied Ir(III) complexes: ***m***, ***f*-ct14**, ***m***, ***f*-ct15** and ***m*-ct16**.

© 2025 The Author(s). Angewandte Chemie International Edition published by Wiley-VCH GmbH

15213773, 2025, 11, Downloaded from https://onlinelibrary.wiley.com/doi/10.1002/anie.202421664 by City University Of Hong Kong, Wiley Online Library on [17/03/2025]. See the Terms and Conditions (https://onlinelibrary.wiley.com/terms-and-conditions) on Wiley Online Library for rules of use; OA articles are governed by the applicable Creative Commons License

ratio of LBH_2^+ vs. $[Ir(COD)(\mu\text{-}Cl)]_2$ from 4:1 to 2:1 and conducted the reaction in the nonpolar solvent at a lowered temperature. This is targeted at the generation of a speculative intermediate with the formula [Ir(COD)(LBH)-(Cl)].[15] After then, heating of this mixture with four equiv. of LAH_2^+ in *o*-dichlorobenzene at 180 °C gave isolation of ***m*-ct16** as the sole product. Remarkably, we observed no *fac*-isomer in this product solution, and upon further refluxing of ***m*-ct16** in 1,2,4-trichlorobenzene in the presence of sodium acetate and *p*-toluene sulfonic acid, confirming the influence of N-mesityl substituents in inhibition of this geometry, most likely by excessive steric encumbrance.

These Ir(III) complexes were next characterized by high-resolution mass analyses, ^{1}H NMR spectroscopies, and most importantly, single-crystal X-ray diffraction studies. Their structural diagrams were depicted in Figures S1–S5 and subjected to closer scrutiny.[16] For ***m*-ct14** and ***m*-t15**, the unique N-mesityl substituted carbene cyclometallation was preferentially located at one "transoid" position with its mesityl group forming π–π contact to the phenyl cyclometalate of the "cisoid" (or central) carbene chelate.[17] In the case of ***m*-ct16**, both N-mesityl appendages took these transoid positions, which are believed to possess the smallest spatial interaction with other N-aryl appendages within the molecule. As to the *fac*-isomers, namely, ***f*-ct14** and ***f*-ct15**, all three N-aryl appendages were found to be located at the spatially confined, triangular sites of the octahedral framework. The H···H contacts between the *o*-methyl group of mesityl entity and adjacent N-phenyl appendages were measured to be ~2.42–2.46 Å, while the N-mesityl group is also tilting away from the adjacent N-phenyl appendages for relieving steric hindrance. Importantly, the shortest non-bonding distance is close to the sum of the Van der Waals radius of H atoms, indicating the severe steric repulsion. In sharp contrast, homoleptic carbene derivatives such as ***f*-ct1a** and ***f*-Ir(tBpp)$_3$** (with solely the N-phenyl appendages) exhibited less conformational distortion and larger H···H contact of 2.48–4.43 Å,[18] respectively. This means that if any additional N-phenyl appendage was replaced by the N-mesityl group, the resulting structure would experience an increased steric repulsion at this triangular region, giving severe destabilization. This hypothesis could be employed to account for the lack of *fac*-counterpart (i.e., ***f*-ct16**) during their initial synthesis, as well as the failure in getting homoleptic Ir(III) complexes with three N-mesityl substituted carbene cyclometalates or carbene chelates carrying other class of bulky appendage. Moreover, this observation is also reminiscent of a partial *fac*-to-*mer* conversion that occurred during heating of ***f*-IrS^{iPr}**,[19] which also possessed the relatively bulky N-isopropyl substituents.

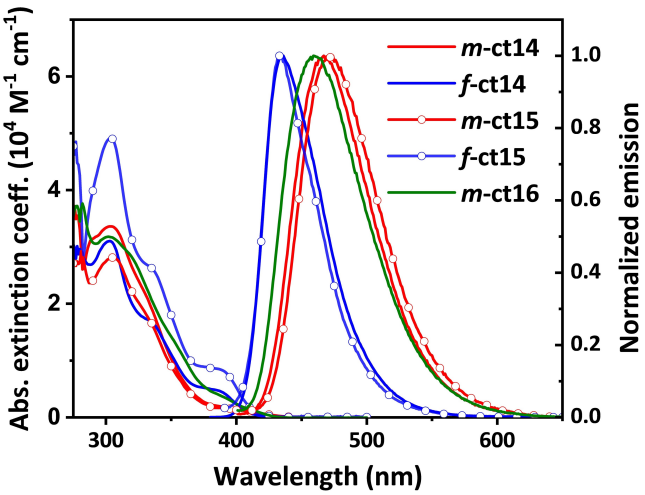

Figure 1. Absorption and emission spectra of studied Ir(III) complexes with a conc. of 10^{-5} M in toluene at RT.

Photophysical characteristics. The absorption spectra of studied Ir(III) complexes were recorded in toluene, and the respective spectra and numerical data are given in Figure 1 and Table 1, respectively. The obtained spectra have reflected the structural properties of these Ir(III) complexes. They showed intense absorption bands at the region above ~350 nm, which are assigned to the spin-allowed ligand-

Table 1: Photophysical data of relevant Ir(III) complexes recorded in toluene at RT.

Complex	abs λ_{max} (nm)[a]	em λ_{max} (nm)[a]	FWHM (nm)[b]	PLQY (%)[c,d]	τ_{obs} (μs)[c]	τ_{rad} (μs)[c]	k_r (10^5 s^{-1})	k_{nr} (10^5 s^{-1})
***m*-ct14**	305 (3.3), 335 (1.9)	467	69	86	0.79	0.91	10.96	1.78
***f*-ct14**	303 (3.1), 338 (1.6), 387 (0.5)	434	51	82	0.79	0.96	10.42	2.24
***m*-ct15**	305 (2.8), 335 (1.6)	472	70	80	0.84	1.05	9.52	2.38
***f*-ct15**	304 (4.9), 336 (2.6), 389 (0.8)	434	48	78	0.75	0.96	10.43	2.94
***m*-ct16**	303 (3.2), 321 (2.8), 354 (1.2)	459	73	78	0.62	0.79	12.59	3.65

[a] Recorded in degassed toluene at a conc. of 10^{-5} M at RT; extinction coefficient (ε) is given in parentheses with a unit of 10^4 M^{-1}·cm^{-1}. [b] Full width at half maximum. [c] Recorded in degassed toluene at a conc. of 10^{-5} M. [d] Coumarin 102 (C102) in methanol (PLQY = 87% and λ_{max} = 480 nm) was employed as standard.

© 2025 The Author(s). Angewandte Chemie International Edition published by Wiley-VCH GmbH

15213773, 2025, 11, Downloaded from https://onlinelibrary.wiley.com/doi/10.1002/anie.202421664 by City University Of Hong Kong, Wiley Online Library on [17/03/2025]. See the Terms and Conditions (https://onlinelibrary.wiley.com/terms-and-conditions) on Wiley Online Library for rules of use; OA articles are governed by the applicable Creative Commons License

centered (LC) ππ* transitions of the cyclometalating chelate, whereas the weaker bands at the lower energy region beyond 370 nm are attributed to the metal-to-ligand charge transfer (MLCT) transitions. Notably, the *fac*-isomers ***f*-ct14** and ***f*-ct15** seemed to exhibit an increased absorption intensity of this MLCT band in reference to their *mer*-counterparts ***m*-ct14** and ***m*-ct15**. This behaviour is common for the *fac*-arranged Ir(III) carbene complexes. Alternatively, the derivative ***m*-ct16** possesses an intermediate intensity in comparison with the MLCT band of other derivatives, presumably owing to the possession of two mesityl substituted chelates in giving more symmetrical structure (vide supra).

Upon excitation, all these Ir(III) complexes showed intense blue emission in degassed toluene at RT. The associated photoluminescence and parameters are also given in Figure 1 and Table 1 for scrutiny. The *fac*-isomers (***f*-ct14** and ***f*-ct15**) exhibit blue-shifted luminescence with peak max. located at 434 and 434 nm, in reference to the *mer*-derivatives with peak max. at 467, 472 and 459 nm for ***m*-ct14**–***m*-ct16**, respectively. Moreover, they have shown high photoluminescence quantum yield (PLQY), radiative lifetime slightly lower than 1 μs, and lower non-radiative decay rate constant, confirming their good phosphorescent efficiencies. In addition, all the *m*-complexes showed larger full width at half maximum (FWHM) of 69 ~ 73 nm in comparison to that of *f*-derivatives at 48 ~ 51 nm, due to the asymmetrical arrangement of carbene cyclometalates and increased charge transfer contributions for *m*-derivatives at the excited states.[20] Their spectra were also recorded in CH_2Cl_2 for assessing solvent effects. As shown in Figure S6 and Table S1, there is no visible change in absorption bands, but their emissions had undergone obvious red shifting and given larger FWHM in reference to those recorded in toluene. These properties agreed with the better stabilization of the excited molecules with greater charge separation in the solvents of higher polarity.[21]

Electrochemical and thermal properties. Our TG analysis indicated the existence of high stability with T_d of > 390 °C, i.e., the temperature at which a weight loss of 5 % was recorded (Figure S7). Moreover, all the *mer*-isomers seemed to be less stable upon dissolution in $CDCl_3$ ($CHCl_3$) for a longer period. This is shown by the obvious change of color for the specific solution, and it can be interpreted as the (chloro) radical induced oxidative decomposition, which is common to many organometallic derivatives. Next, their redox behaviours were investigated using cyclic voltammetry (CV) in acetonitrile. As shown in Figure S8, the *fac*-complexes show more anodic shifted oxidation potentials (***f*-ct14**: 0.35 V and ***f*-ct15**: 0.34 V) than that of *mer*-isomers (***m*-ct14**: 0.21 V, ***m*-ct15**: 0.19 V, and ***m*-ct16**: 0.26 V), respectively. The cathodic shift of oxidation potential from *fac*- to *mer*-isomers agreed with the relevant literature reports.[22] Moreover, the oxidation peak onset of ***m*-ct16** with two LA cyclometalates with electron deficient cyano substituent was found to be stabilized by ~0.05 V compared to their analogues (***m*-ct14** and ***m*-ct15**), each with only one LA chelate. Finally, the HOMO gaps were estimated by the oxidation onsets taking ferrocene as the reference. Next, their LUMO levels were determined through their HOMO data and experimentally determined optical energy gap. These data are listed in Table 2 as they are highly critical for proposing the initial OLED architectures mentioned in the device session.

Theoretical Investigation. To improve our understanding of the photophysical properties of the studied Ir(III) complexes in their singlet (S_1) and triplet (T_1) excited states, the time-dependent density functional theory (TD-DFT) calculations and the natural transition orbitals (NTOs) analysis were performed.[23] In general, the TD-DFT predictions on the vertical excitation energies and radiative lifetime are quite good (see Supporting Information), here in, we focus only on the NTO results.

The electron density distributions of the occupied NTOs located at both the Ir(III) metal center and the carbene chelates (π orbitals), with contributions of Ir(III) center being > 30 % (Figure 2 and Figure S9). In contrast, the virtual NTOs were mainly situated at the carbene chelates (π* orbitals), with the contribution of the Ir(III) center decreased to ~5 %. These results demonstrate that all the studied Ir(III) complexes exhibit MLCT characters. The inter-fragment charge transfer (IFCT) analysis of all the optimized S_0 and T_1 structures in the $S_0 \rightarrow T_1$ transition for the studied Ir(III) complexes was conducted using Multiwfn software.[24] This analysis quantifies the contributions of the transition processes, including MLCT, ligand-to-metal charge transfer (LMCT), ligand-to-ligand charge transfer (LLCT), ligand-centered (LC), and metal-centered (MC) characters. The IFCT results for the $S_0 \rightarrow T_1$ transition, calculated at the S_0 structures of the Ir(III) complexes, show a combination of MLCT, LLCT and LC characters (34.4 %, 27.0 % and 33.7 % for ***m*-ct14**; 34.5 %, 26.6 % and 34.3 % for

Table 2: Voltammetric data, experimental energy gaps and decomposition temperature (T_d) of the studied Ir(III) complexes at RT.

Complex	E^{ox}_{onset} (V)[a]	E_{HOMO} (eV)[b]	E^{opt}_{g} (eV)[c]	E_{LUMO} (eV)[d]	T_d (°C)[e]
***m*-ct14**	0.21	−5.01	2.93	−2.08	391
***f*-ct14**	0.35	−5.15	3.04	−2.11	421
***m*-ct15**	0.19	−4.99	2.90	−2.09	398
***f*-ct15**	0.34	−5.14	3.05	−2.09	408
***m*-ct16**	0.26	−5.06	2.98	−2.08	427

[a] Electrochemical potentials were measured in a 0.1 M acetonitrile solution of $TBAPF_6$. referenced to the Fc/Fc^+ couple; E^{ox}_{onset} is the onset potential for the oxidation wave; [b] HOMO = −(E^{ox}_{onset} + 4.8); [c] Energy gap = 1240/[PL_{onset} (nm)]; [d] LUMO=HOMO + energy gap; [e] Temperature with a 5 % loss in weight; T_d is recorded under N_2 flow.

© 2025 The Author(s). Angewandte Chemie International Edition published by Wiley-VCH GmbH

15213773, 2025, 11, Downloaded from https://onlinelibrary.wiley.com/doi/10.1002/anie.202421664 by City University Of Hong Kong, Wiley Online Library on [17/03/2025]. See the Terms and Conditions (https://onlinelibrary.wiley.com/terms-and-conditions) on Wiley Online Library for rules of use; OA articles are governed by the applicable Creative Commons License

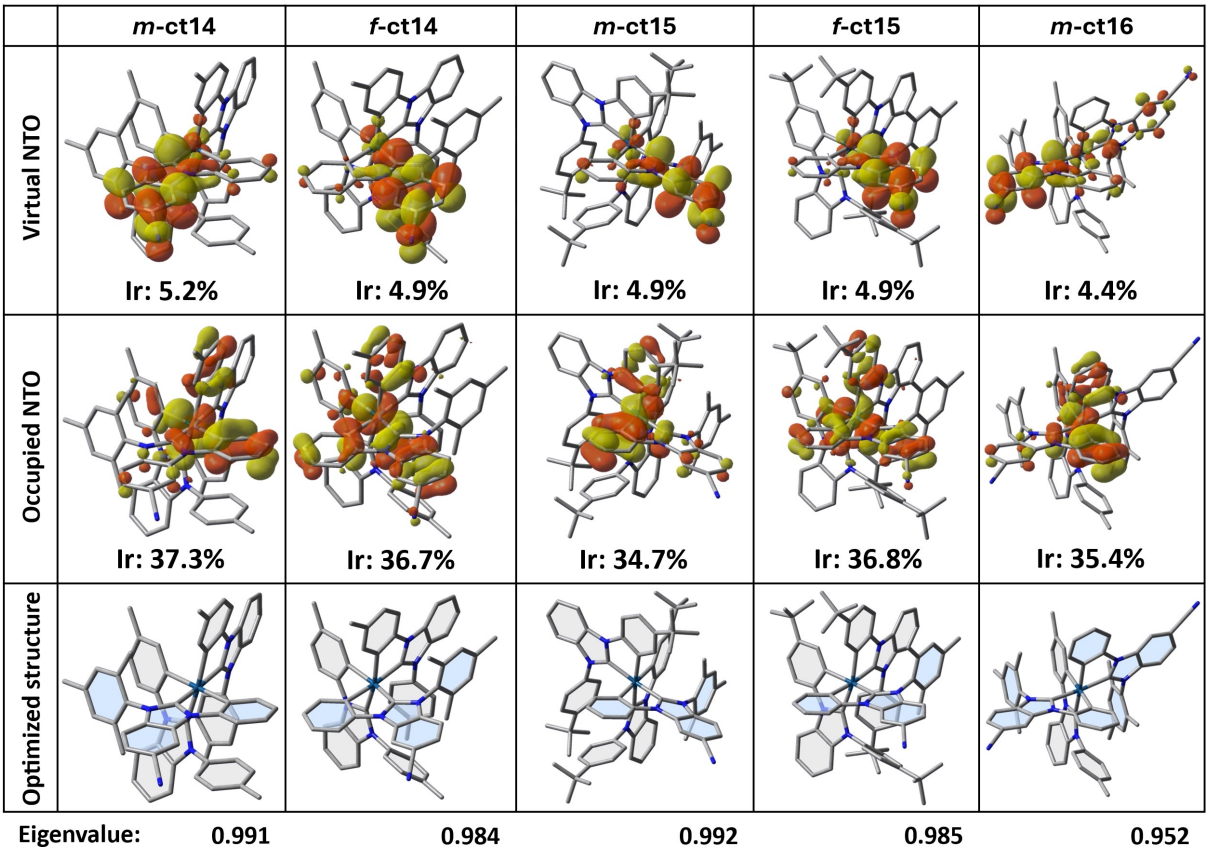

Figure 2. The dominant natural transition orbital (NTO) pairs and their eigenvalues represent the T_1 excited states of the investigated Ir(III) complexes at their geometrically optimized S_0 structures, including the contribution of the Ir center to the NTOs.

f*-ct14**; 33.0 %, 23.3 % and 39.1 % for ***m*-ct15**; 35.3 %, 27.8 % and 32.4 % for ***f*-ct15**, 32.6 %, 30.0 % and 33.2 % for ***m*-ct16**; Table S2). A higher proportion of MLCT generally indicates a quicker radiative transition, and the influence of MLCT on the emission of ***m- and ***f***- isomers is significant. The calculated MLCT contributions for ***m*-ct14** and ***f*-ct14** are 34.4 % and 34.5 % at their respective S_0 structures, changing to 33.8 % and 28.5 % at their respective T_1 structures (Table S2). This decrease may potentially explain the larger experimental k_r value found for ***m*-ct14** (10.9×10^5 s^{-1}; Table 1) compared with ***f*-ct14** (10.4×10^5 s^{-1}). For ***m*-ct15**, the computed MLCT contributions are 33.0 % (at the S_0 structure) and 30.4 % (at the T_1 structure), both of which are smaller than those of ***f*-ct15** (35.3 % at the S_0 structure and 32.9 % at the T_1 structure). This aligns with the smaller experimental k_r value observed for ***m*-ct15** (9.5×10^5 s^{-1}; Table 1) compared to ***f*-ct15** (10.4×10^5 s^{-1}). Although ***m*-ct16** exhibits the smallest MLCT contribution (32.6 %) among all the studied Ir(III) complexes at the S_0 structure, it has the largest MLCT contribution (33.9 %) at T_1 structure. The significant MLCT contribution correlates well with the experimental observation that ***m*-ct16** has the highest k_r value (12.59×10^5 s^{-1}) among all studied Ir(III) complexes.

Device fabrication and characterization. Given their superiority in photoluminescent quantum yield, blue emission, fast radiative decay and excellent thermal stability, ***f*-ct14**, ***f*-ct15** and ***m*-ct16** were selected as both dopant emitters and sensitizers in the fabrication of vacuum-deposited OLEDs, to which the device architecture (**Device I**) consists of indium tin oxide (ITO)/1,4,5,8,9,11-hexaazatriphenylenehexacarbonitrile (HAT-CN, 5 nm)/1,1-bis [(di-4-tolylamino) phenyl]cyclohexane (TAPC, 30 nm)/4,4',4"-tris-(carbazol-9-yl) triphenylamine (TCTA, 15 nm)/3,3-di-(9H-carbazol-9-yl) biphenyl (mCBP, 10 nm)/2,8-bis (diphenylphosphoryl) dibenzo [b,d] furan (PPF): ***f*-ct14**, ***f*-ct15** and ***m*-ct16** (25 nm)/PPF (10 nm)/1-[4-(10-([1,1-biphenyl]-4-yl)-anthracen-9-yl) phenyl]-2-ethyl-1H-benzo [d] imidazole (ANT-BIZ, 30 nm)/8-hydroxyquinolinolatolithium (Liq, 2 nm)/Al (100 nm). To all devices, HAT-CN and Liq served as the hole-injection and electron-injection layers, respectively. TAPC and TCTA functioned as both the hole-transporting and hole-injecting layers, while mCBP and ANT-BIZ were employed as electron-blocking and electron-transporting layers, respectively. Additionally, PPF was selected as both the host material and hole-blocking layer for its high triplet energy ($E_T = 3.1$ eV). In seeking optimized performances, the doping concentrations of the dopants, i.e., ***f*-ct14**, ***f*-ct15** and ***m*-ct16**, were varied from 5 % to 40 %. The device architecture, along with structural drawings of all employed materials and associated energy levels, are depicted in Figure 3a and Figure S10.

© 2025 The Author(s). Angewandte Chemie International Edition published by Wiley-VCH GmbH

15213773, 2025, 11, Downloaded from https://onlinelibrary.wiley.com/doi/10.1002/anie.202421664 by City University Of Hong Kong, Wiley Online Library on [17/03/2025]. See the Terms and Conditions (https://onlinelibrary.wiley.com/terms-and-conditions) on Wiley Online Library for rules of use; OA articles are governed by the applicable Creative Commons License

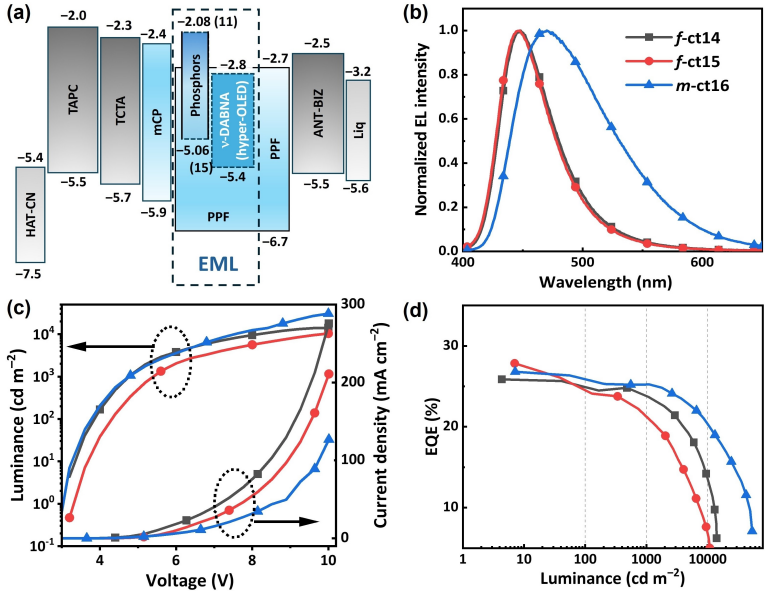

Figure 3. Performances of OLED devices with ***f*-ct14**, ***f*-ct15** and ***m*-ct16** as the dopant at a concentration of 30 wt%. (a) Device architecture; (b) EL spectra measured at a current density of 10 mA cm^{-2}; (c) Corresponding current density-voltage-luminance (*J*–*V*–*L*) characteristics; (d) EQE versus luminance of devices.

Figures S11–13 presented the device characteristics with dopants ***f*-ct14**, ***f*-ct15** and ***m*-ct16** at varied concentrations. As expected, the higher concentration of dopant phosphors is beneficial in improving the current efficiency (CE) as well as the external quantum efficiency (EQE). Such phenomenon can be understood in terms of the shallow HOMO energy levels of the dopants (−5.14 to −5.15 eV) vs that of PPF (−6.7 eV). Consequently, it induced severe hole-trapping within the emissive layer (EML), and it can be reduced at the higher doping ratios. Notably, the turn-on voltages (Table S4) gradually decrease at higher doping concentrations, and similar trends are also observed in many literature precedents.[25] Additionally, the current density was significantly improved to 19.6, 16.3 and 46.5 cd A^{-1} at the practical luminance of 1000 cd m^{-2}, for ***f*-ct14**, ***f*-ct15** and ***m*-ct16**, respectively, which can be attributed to much balanced carrier transport characteristics. Despite a slight bathochromic shift observed at higher doping concentrations, likely caused by the increased ππ stacking interaction between host and dopant molecules, these OLED devices still delivered promising performances. Finally, the champion devices were obtained with dopant at 30 wt%, to which the corresponding device characteristics and detailed parameters were depicted in Figure 3 and Table 3, respectively.

Notably, ***f*-ct14** and ***f*-ct15** based devices exhibited deep-blue emission peaking at 448 and 446 nm, with narrowband FWHMs of 52 and 51 nm, respectively. The Commission Internationale de L'Eclairage (CIE) coordinates are recorded to be (0.151, 0.088) and (0.150, 0.082) for ***f*-ct14** and ***f*-ct15**, respectively, closely aligning with the BT.2020 specification (0.131, 0.046) for blue light.[26] Additionally, these devices also demonstrated low turn-on voltage of 3.2 and 3.3 eV, high maximum EQE of 25.9% and 27.9%, CE of 22.6 cd·A^{-1} and 21.2 cd·A^{-1}, and power efficiencies (PE) of 22.2 lm·W^{-1} and 18.5 lm·W^{-1}, respectively. These performance metrics can be attributed to balanced carrier transport and faster Förster resonance energy transfer (FRET) from host to dopant. Remarkably, they also achieved impressive EQE of 23.8% and 21.4% at practical brightness of 1000 cd m^{-2}, demonstrating the great potential of these phosphors in OLED applications. The broadened FWHMs of the *mer*-isomers may be due to the asymmetrical arrangement of carbene cyclometalates and increased participation of ligand-to-ligand charge transfer contributions at the excited states. Moreover, the PPF host material with greater polarity would also increase the bandwidth of electroluminescence. Most importantly, the ***m*-ct16** based OLED device showed efficient blue emission with a peak

Table 3: EL Performances of devices using ***f*-ct14**, ***f*-ct15** and ***m*-ct16** at the optimal ratio of 30 wt%.

Device	V_{on} (V)	EQE (%)[a]	CE (cd·A^{-1})[a]	PE (lm·W^{-1})[a]	λ_{EL} (nm)[b]	FWHM (nm)[b]	CIE$_{(x,y)}$[b]
***f*-ct14**	3.2	25.9/23.8/19.0	22.6/19.6/15.4	22.2/13.1/7.5	448	52	0.151, 0.088
***f*-ct15**	3.3	27.9/21.4/13.2	21.2/16.3/10.1	18.5/9.5/4.2	446	51	0.150, 0.082
***m*-ct16**	3.0	26.8/25.2/22.8	53.4/46.5/42.7	52.4/31.0/20.7	470	92	0.182, 0.267

[a] The maximum, and the value recorded at 1000 cd m^{-2} and 5000 cd m^{-2}; [b] those recorded at a current density of 10 mA cm^{-2}.

© 2025 The Author(s). Angewandte Chemie International Edition published by Wiley-VCH GmbH

15213773, 2025, 11, Downloaded from https://onlinelibrary.wiley.com/doi/10.1002/anie.202421664 by City University Of Hong Kong, Wiley Online Library on [17/03/2025]. See the Terms and Conditions (https://onlinelibrary.wiley.com/terms-and-conditions) on Wiley Online Library for rules of use; OA articles are governed by the applicable Creative Commons License

maximum of 470 nm, and max. EQE of 26.8 %, together with EQE of 25.2 % and 22.8 % at luminance of 1000 and 5000 cd m^{-2}, respectively. The alleviated efficiency roll-offs at higher current densities could be rationalized by its lowered emission energy and the presence of two bulky mesityl groups, which greatly reduced host-dopant ππ-stacking interactions.

Next, the photophysical characteristics of ***f*-ct14**, ***f*-ct15** and ***m*-ct16** in doped PPF films at a concentration of 30 wt % were investigated. As shown in Figure S14 and Table S5, the PL peaks of ***f*-ct14**, ***f*-ct15** and ***m*-ct16** occurred at 450, 451 and 478 nm with high quantum yields of over 80 %, which were consistent with their EL performances. Given the nearly identical emission profiles, the slightly higher max. EQE of ***f*-ct15** based OLED can be ascribed to the higher PLQY of doped thin film.

Recently, both the hyperfluorescence OLED (HF-OLED)[27] and hyperphosphorescence OLED (HP-OLED)[28] have gained popularity in the fabrication of blue OLEDs. These devices have achieved narrowband emission via conveying excitation energy from the TADF or phosphorescent sensitizers to terminal multiple resonance TADF (MR-TADF) emitters through efficient FRET process. To avoid the deteriorated energy loss channels such as the Dexter Energy Transfer (DET) process,[29] which is a short-range energy transfer process and requires the direct overlap of electron cloud of both the donors (or sensitizers) and acceptors (or terminal emitters), and the rate constant of DET process would decay exponentially upon increasing the distances of donors and acceptors.[30] Hence, it can be experimentally suppressed by the installation of the bulky group (s) on both materials and reducing the concentration of terminal emitters.[31] Accordingly, with both the high quantum yields and fast radiative rates, our Ir(III) carbene complexes are undouble the ideal candidates in serving as the designated sensitizers.[32]

In this work, hyper-OLEDs were then fabricated using ***f*-ct14**, ***f*-ct15**, and ***m*-ct16** as the dopant sensitizers and N^7,N^7,N^{13},N^{13},5,9,11,15-octaphenyl-5,9,11,15-tetrahydro-5,9,11,15-tetraaza-19b,20b-diboradinaphtho [3,2,1-*de*:1′,2′,3′-*jk*] pentacene-7,13-diamine (ν-DABNA) as narrowband terminal emitter.[33] The corresponding devices with configuration of ITO/HAT-CN (5 nm)/TAPC (30 nm)/TCTA (15 nm)/mCBP (10 nm)/PPF : 30 wt % phosphors : x wt % ν-DABNA (25 nm)/PPF (10 nm)/ANT-BIZ (30 nm)/Liq (2 nm)/Al (100 nm) were constructed. These OLED characteristics are depicted in Figure 4 and Figure S15 with doping concentrations of ν-DABNA being 1 wt % and 2 wt %, respectively.

As depicted in Table 4, the detailed metric parameters of all hyper-OLED devices are included. As expected, all the devices exhibited a narrowed FWHM of 19 nm with the peak wavelength located at ~472 nm, which resembled that of the reference device.[34] Notably, max. EQEs of 32.7 %, 30.2 % and 32.9 % were obtained for ***f*-ct14**, ***f*-ct15** and ***m*-ct16**, respectively. The significantly enhanced EQEs at their maximum and practical luminance (i.e., at 1000 and 5000 cd m^{-2}) compared to that of the control device, can be rationalized by the ultra-fast radiative decay to reduce the triplet exciton density, and hence mitigate DET process. Remarkably, the device with sensitizer ***m*-ct16** exhibited the best performance among all hyper-OLEDs present in this investigation. Moreover, it exhibited lowered driving voltages in achieving luminance of 1000 cd·m^{-2} (4.4 V) and 5000 cd·m^{-2} (6.0 V), which significantly diminished the emission quenching occurred at the higher driving voltages.

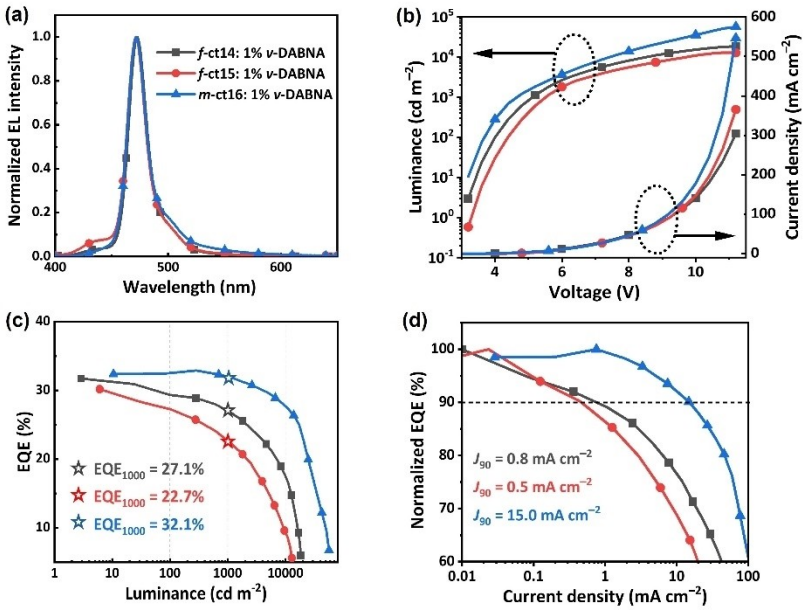

Figure 4. Performances of hyper-OLED devices with ***f*-ct14**, ***f*-ct15** and ***m*-ct16** (30 wt %) as sensitizers and υ-DABNA (1 wt %) as terminal emitter. (a) EL spectra measured at a current density of 10 mA·cm^{-2}; (b) Corresponding current density-voltage-luminance (*J*–*V*–*L*) characteristics; (c) EQE versus luminance of devices; (d) Normalized EQE versus current density of devices.

© 2025 The Author(s). Angewandte Chemie International Edition published by Wiley-VCH GmbH

15213773, 2025, 11, Downloaded from https://onlinelibrary.wiley.com/doi/10.1002/anie.202421664 by City University Of Hong Kong, Wiley Online Library on [17/03/2025]. See the Terms and Conditions (https://onlinelibrary.wiley.com/terms-and-conditions) on Wiley Online Library for rules of use; OA articles are governed by the applicable Creative Commons License

Notably, ***m*-ct16** sensitizer exhibited the most red-shifted emission and relatively shallower HOMO energy level. Benefiting from the lowered excitation energy of ***m*-ct16** as well as its higher lying HOMO vs. that of ν-DABNA, the corresponding hyper-OLED exhibited significantly improved performances. Additionally, the fast radiative decay of ***m*-ct16** in PPF host and decreased triplet exciton density on ν-DABNA allowed the hyper-OLED to display suppressed efficiency roll-offs at higher brightness, which mitigated unwanted non-radiative decay as well as triplet-triplet annihilation (TTA) or triplet-polaron annihilation (TPA) within the EML. Most importantly, as shown in Figures 4c, d and TOC illustration, it transcended the suppressed efficiency roll-off of their PhOLED counterpart, giving an excellent figure of merit (FOM),[35] i.e., EQE_{1000} of 32.1 % (EQE recorded at 1000 $cd \cdot m^{-2}$) and J_{90} of 15.0 mA cm^{-2} (current density recorded at 90 % of max. EQE). This result is unusual for blue TADF OLEDs and associated hyper-OLEDs. As shown in Table S6, our performance data are superior to those of the reported hyper-OLED devices including our earlier work on ***f*-ct1b** (EQE_{1000} = 24.5 % and J_{90} = 3.2 mA cm^{-2}),[18a] ***f*-ct5mix** (EQE_{1000} = 25.5 % and J_{90} = 2.5 mA cm^{-2}),[18c] ***f*-ct9b** (EQE_{1000} = 25.5 % and J_{90} = 3.0 mA cm^{-2}),[11d] and ***f*-Ir($L_{6F}B$)$_3$** (EQE_{1000} = 23.0 % and J_{90} = 1.5 mA cm^{-2}),[28c] all with the common terminal emitter ν-DABNA. Probably, the improvement in efficiencies could be facilitated by the N-mesityl substituent of associated carbene chelates. In addition, our device also showed impressive performance at high luminance, i.e., EQE = 27.7 % at 10000 $cd \cdot m^{-2}$ and EQE = 23.1 % at 20000 $cd \cdot m^{-2}$. Next, the OLED stability was examined with more stable architecture and materials: ITO/ HATCN (5 nm)/TBBD (30 nm)/*o*-SFAF (15 nm)/ mCBP (15 nm)/EML (25 nm)/SitrzCZ2 (20 nm)/ANT-BIZ (30 nm)/Liq/Al.[36] As shown in Figure S16, the corresponding PhOLED achieved a LT_{50} of 21 hours at an initial luminance (L_0) of 1000 $cd \cdot m^{-2}$. Additionally, facilitated by the fast radiative decay and lowered excitation energy of ***m*-ct16**, the hyper-OLED exhibited a LT_{50} of 52 hours under the same condition, both statistics are better than its Ir(III) carbene precedents ***f*-ct9b** (λ_{EL} = 468 nm, LT_{50} = 7 h with L_0 = 1000 $cd \cdot m^{-2}$)[11d] and ***f*-ct8c** (λ_{EL} = 472 nm, LT_{50} = 53 h with L_0 = 500 $cd \cdot m^{-2}$).[9c] These performances have proved their potentials in serving as the dopant sensitizers for blue hyper-OLED devices.

Summary and Conclusions

With the goal of making authentic blue OLED phosphors, we synthesized two distinctive classes of heteroleptic Ir(III) carbene complexes, namely, ***m*, *f*-ct14**, ***m*, *f*-ct15** and ***m*-ct16**. By varying the stoichiometric ratio of N-mesityl substituted asymmetrical pro-chelate LAH_2^+ vs. the symmetrical carbene counterparts LBH_2^+ (or LCH_2^+) from 1:2 to 2:1, we obtained a mixture of ***m*, *f*-ct14** and ***m*, *f*-ct15** and, then, solely the *mer*-substituted derivative ***m*-ct16**. The successful isolation of these Ir(III) emitters breaks the myth that carbene with N-mesityl appendage cannot be employed to afford the stable tris-bidentate Ir(III) complexes. Next, single-crystal X-ray diffraction study confirmed their structural identifications, while photophysical investigation revealed deep-blue to sky-blue emission with $\Phi_{PL} \geq 78$ % and short $\tau_{rad} \leq 1.05$ μs in degassed toluene with peak maximum located at 467, 472 and 459 nm for ***m*-ct14**–***m*-ct16**, and at 434 nm for both ***f*-ct14** and ***f*-ct15**, respectively. The ***f*-ct14** and ***f*-ct15** based OLED devices exhibited true blue emission with $CIE_{x,y}$ coordinates of (0.151, 0.088) and (0.150, 0.082), and max. EQEs of 25.9 % and 27.9 %, respectively, while the ***m*-ct16** based device exhibited sky-blue emission with $CIE_{x,y}$ coordinates of (0.182, 0.267) and comparable max. EQE of 26.8 %. Furthermore, hyper-OLED devices were also attempted using these Ir(III) carbene emitters as sensitizers and ν-DABNA as terminal emitter, giving narrowband emission at ~471 nm and with FWHMs of 19 nm and high max. EQEs of 32.7–32.9 %. Remarkably, the device based on ***m*-ct16** delivered low driving voltages (i.e., 4.4 V at luminance of 1000 $cd \cdot m^{-2}$ and 6.0 V at 5000 $cd \cdot m^{-2}$) and extremely suppressed efficiency roll-off (i.e., EQE = 32.1 % at 1000 $cd \cdot m^{-2}$ and EQE = 27.7 % at 10000 $cd \cdot m^{-2}$), and an excellent FOM for the blue OLED devices, i.e., EQE_{1000} of 32.1 % and J_{90} of 15.0 mA cm^{-2}. Hence, these emitters have not only confirmed the capability of N-mesityl group of carbene cyclometalates in fine-controlling molecular geometries, but also provided a feasible design of blue OLED devices with superior performance characteristics.

Supporting Information

Details of chelate syntheses, single crystal X-ray diffraction analyses, supportive photophysical and electrochemical data, computational study and TD-DFT results, supportive OLED performance data of all studied Ir(III) metal complexes, and ^{1}H NMR spectra of the studied Ir(III) complexes.

Acknowledgements

Funding and research grants of this work are provided by the University Grants Council (CityU 11304221, 11312722 and 11305224) of Hong Kong SAR for Y.C. and the National Natural Science Foundation of China (grant No. 52130308) and the Shenzhen Science and Technology Program (grant No. JCYJ20220818095816036 and ZDSYS20210623091813040) for C.Y. The computational studies were carried out using the High-Performance Computing facility, i.e., CityU Burgundy at City University of Hong Kong.

Conflict of Interest

The authors declare no conflict of interest.

© 2025 The Author(s). Angewandte Chemie International Edition published by Wiley-VCH GmbH

15213773, 2025, 11, Downloaded from https://onlinelibrary.wiley.com/doi/10.1002/anie.202421664 by City University Of Hong Kong, Wiley Online Library on [17/03/2025]. See the Terms and Conditions (https://onlinelibrary.wiley.com/terms-and-conditions) on Wiley Online Library for rules of use; OA articles are governed by the applicable Creative Commons License

Data Availability Statement

The data that support the findings of this study are available in the supplementary material of this article.

Keywords: blue light emission · Förster resonance energy transfer · iridium · organic light emitting diodes

[1] G. Hong, X. Gan, C. Leonhardt, Z. Zhang, J. Seibert, J. M. Busch, S. Bräse, *Adv. Mater.* **2021**, *33*, 2005630.

[2] J. M. Ha, S. H. Hur, A. Pathak, J.-E. Jeong, H. Y. Woo, *NPG Asia Mater.* **2021**, *13*, 53.

[3] a) Y. Chi, P.-T. Chou, *Chem. Soc. Rev.* **2010**, *39*, 638–655; b) H. Xiang, J. Cheng, X. Ma, X. Zhou, J. J. Chruma, *Chem. Soc. Rev.* **2013**, *42*, 6128–6185; c) J.-H. Jou, S. Kumar, A. Agrawal, T.-H. Li, S. Sahoo, *J. Mater. Chem. C* **2015**, *3*, 2974–3002; d) W.-P. To, G. Cheng, G. S. M. Tong, D. Zhou, C.-M. Che, *Front. Chem.* **2020**, *8*, 653; e) K. Li, Y. Chen, J. Wang, C. Yang, *Coord. Chem. Rev.* **2021**, *433*, 213755.

[4] a) H. Fu, Y.-M. Cheng, P.-T. Chou, Y. Chi, *Mater. Today* **2011**, *14*, 472–479; b) Y. Im, S. Y. Byun, J. H. Kim, D. R. Lee, C. S. Oh, K. S. Yook, J. Y. Lee, *Adv. Funct. Mater.* **2017**, *27*, 1603007; c) Z. Xu, B. Z. Tang, Y. Wang, D. Ma, *J. Mater. Chem. C* **2020**, *8*, 2614–2642; d) E. Tankeleviciute, I. D. W. Samuel, E. Zysman-Colman, *J. Phys. Chem. Lett.* **2024**, *15*, 1034–1047.

[5] J. Jiang, J. Y. Lee, *Mater. Today* **2023**, *68*, 204–233.

[6] a) Y. X. Hu, J. Miao, T. Hua, Z. Huang, Y. Qi, Y. Zou, Y. Qiu, H. Xia, H. Liu, X. Cao, C. Yang, *Nat. Photonics* **2022**, *16*, 803–810; b) Q. Li, Y. Wu, Q. Yang, S. Wang, S. Shao, L. Wang, *ACS Appl. Mater. Interfaces* **2022**, *14*, 49995–50003; c) I. S. Park, H. Min, T. Yasuda, *Angew. Chem. Int. Ed.* **2022**, *61*, e202205684; d) S. M. Pratik, V. Coropceanu, J.-L. Brédas, *Chem. Mater.* **2022**, *34*, 8022–8030; e) J. Jin, S. Wang, H. Jiang, L. Wang, W.-Y. Wong, *Adv. Opt. Mater.* **2024**, *12*, 2302354.

[7] a) P.-T. Chou, Y. Chi, *Chem. Eur. J.* **2007**, *13*, 380–395; b) C.-W. Lu, Y. Wang, Y. Chi, *Chem. Eur. J.* **2016**, *22*, 17892–17908; c) C. Cebrián, M. Mauro, *Beilstein J. Org. Chem.* **2018**, *14*, 1459–1481; d) A. Bonfiglio, M. Mauro, *Eur. J. Inorg. Chem.* **2020**, *2020*, 3427–3442; e) S. Lee, W.-S. Han, *Inorg. Chem. Front.* **2020**, *7*, 2396–2422; f) H. Amouri, *Chem. Rev.* **2023**, *123*, 230–270; g) M. Hruzd, R. Durand, S. Gauthier, P. le Poul, F. Robin-le Guen, S. Achelle, *Chem. Rec.* **2024**, *24*, e202300335.

[8] a) T. Fleetham, G. Li, J. Li, *Adv. Mater.* **2017**, *29*, 1601861; b) J.-M. Kim, K. Cheong, J. Jiang, S. O. Jeon, W. P. Hong, J. Y. Lee, *Trends Chem.* **2023**, *5*, 267–278; c) G. Li, L. Ameri, B. Dorame, Z.-Q. Zhu, J. Li, *Adv. Funct. Mater.* **2024**, *34*, 2405066.

[9] a) Y. Wu, K.-N. Tong, M. Kuhn, C. Wu, W.-Y. Hung, G. Wei, J. Yan, Y. Chi, X. Zhou, *J. Mater. Chem. C* **2025**, DOI: 10.1039/D4TC04498C; b) J. Yan, Y. Pan, Z.-H. Qu, Z. Xu, K.-C. Law, D.-Y. Zhou, L.-S. Liao, Y. Chi, K.-C. Lau, *Adv. Photon. Res.* **2025**, *6*, 2400151; c) J. Yan, C. Wu, S.-M. Yiu, M. Kuhn, M. Huang, Y. Zhang, X. Zhou, C. Yang, G. Wei, Y. Chi, *Adv. Opt. Mater.* **2025**, *13*, 2402332.

[10] a) Y. Chi, T.-K. Chang, P. Ganesan, P. Rajakannu, *Coord. Chem. Rev.* **2017**, *346*, 91–100; b) G. Ni, J. Yan, Y. Wu, F. Zhou, P.-T. Chou, Y. Chi, *Inorg. Chem. Front.* **2023**, *10*, 1395–1401; c) C. Wu, K. Shi, S. Li, J. Yan, Z.-Q. Feng, K.-N. Tong, S.-W. Zhang, Y. Zhang, D. Zhang, L.-S. Liao, Y. Chi, G. Wei, F. Kang, *EnergyChem.* **2024**, *6*, 100120.

[11] a) S. Haneder, E. Da Como, J. Feldmann, J. M. Lupton, C. Lennartz, P. Erk, E. Fuchs, O. Molt, I. Muenster, C. Schildknecht, G. Wagenblast, *Adv. Mater.* **2008**, *20*, 3325–3330; b) K. Tsuchiya, S. Yagai, A. Kitamura, T. Karatsu, K. Endo, J. Mizukami, S. Akiyama, M. Yabe, *Eur. J. Inorg. Chem.* **2010**, *2010*, 926–933; c) J. Yan, S. F. Wang, C.-H. Hsu, E. H.-C. Shi, C.-C. Wu, P.-T. Chou, S.-M. Yiu, Y. Chi, C. You, I. C. Peng, W.-Y. Hung, *ACS Appl. Mater. Interfaces* **2023**, *15*, 21333–21343; d) Y. Wu, Y. Xin, Y. Pan, S.-M. Yiu, J. Yan, K. C. Lau, L. Duan, Y. Chi, *Adv. Sci.* **2024**, *11*, 2309389; e) J. Yan, T. Nakamura, X. Tan, S.-M. Yiu, R. Mimura, K. Hoshi, X. Zhou, Y. Chi, H. Sasabe, J. Kido, *Chem. Eng. J.* **2024**, *488*, 150791.

[12] T. Lv, Z. Wang, J. You, J. Lan, G. Gao, *J. Org. Chem.* **2013**, *78*, 5723–5730.

[13] W. Huang, J. Guo, Y. Xiao, M. Zhu, G. Zou, J. Tang, *Tetrahedron* **2005**, *61*, 9783–9790.

[14] a) F. Monti, M. G. I. La Placa, N. Armaroli, R. Scopelliti, M. Grätzel, M. K. Nazeeruddin, F. Kessler, *Inorg. Chem.* **2015**, *54*, 3031–3042; b) F. Zhang, C. Si, D. Wei, S. Wang, D. Zhang, S. Li, Z. Li, F. Zhang, B. Wei, G. Cao, B. Zhai, *Dyes Pigm.* **2016**, *134*, 465–471; c) H. Na, L. M. Cañada, Z. Wen, J. I. C. Wu, T. S. Teets, *Chem. Sci.* **2019**, *10*, 6254–6260; d) L. M. Cañada, J. Kölling, T. S. Teets, *Polyhedron* **2020**, *178*, 114332.

[15] a) A. G. Tennyson, E. L. Rosen, M. S. Collins, V. M. Lynch, C. W. Bielawski, *Inorg. Chem.* **2009**, *48*, 6924–6933; b) V. Adamovich, S. Bajo, P.-L. T. Boudreault, M. A. Esteruelas, A. M. López, J. Martín, M. Oliván, E. Oñate, A. U. Palacios, A. San-Torcuato, J.-Y. Tsai, C. Xia, *Inorg. Chem.* **2018**, *57*, 10744–10760; c) W. J. Kerr, G. J. Knox, M. Reid, T. Tuttle, *Chem. Sci.* **2021**, *12*, 6747–6755; d) L. Zhou, D. Zhang, J. Hu, Y. Wu, J. Geng, X. Hu, *Organometallics* **2021**, *40*, 2643–2650; e) S. Min, J. Baek, J. Kim, H. J. Jeong, J. Chung, K. Jeong, *JACS Au* **2023**, *3*, 2912–2917.

[16] CCDC Deposition Numbers 2363049 (***m*-ct14**), 2333865 (***f*-ct14**), 2363050 (***m*-ct15**), 2363053 (***f*-ct15**) and 2370770 (***m*-ct16**) contain the supplementary crystallographic data for this paper. These data are provided free of charge by the joint Cambridge Crystallographic Data Centre and Fachinformationszentrum Karlsruhe Access Structures service www.ccdc.cam.ac.uk/structures.

[17] Transoid and cisoid indicated the outer and inner coordination units that took the meridional dispositions of octahedral geometry.

[18] a) J. Yan, D.-Y. Zhou, L.-S. Liao, M. Kuhn, X. Zhou, S.-M. Yiu, Y. Chi, *Nat. Commun.* **2023**, *14*, 6419; b) J. Yan, Y. Pan, I. C. Peng, W.-Y. Hung, B. Hu, G. Ni, S.-M. Yiu, Y. Chi, K. C. Lau, *Inorg. Chem. Front.* **2024**, *11*, 2413–2426; c) J. Yan, C. Wu, K.-N. Tong, F. Zhou, Y. Chen, Y. Pan, G. Xie, Y. Chi, K.-C. Lau, G. Wei, *Small Methods* **2024**, *8*, 2301555.

[19] B.-S. Yun, S.-Y. Kim, J.-H. Kim, H.-J. Son, S. O. Kang, *J. Mater. Chem. C* **2021**, *9*, 4062–4069.

[20] a) J. Lee, H.-F. Chen, T. Batagoda, C. Coburn, P. I. Djurovich, M. E. Thompson, S. R. Forrest, *Nat. Mater.* **2016**, *15*, 92–98; b) J. Yan, Q. Xue, H. Yang, S.-M. Yiu, Y.-X. Zhang, G. Xie, Y. Chi, *Inorg. Chem.* **2022**, *61*, 8797–8805; c) J. Yan, Z.-H. Qu, D.-Y. Zhou, S.-M. Yiu, Y. Qin, X. Zhou, L.-S. Liao, Y. Chi, *ACS Appl. Mater. Interfaces* **2024**, *16*, 3809–3818.

[21] K.-Y. Liao, C.-W. Hsu, Y. Chi, M.-K. Hsu, S.-W. Wu, C.-H. Chang, S.-H. Liu, G.-H. Lee, P.-T. Chou, Y. Hu, N. Robertson, *Inorg. Chem.* **2015**, *54*, 4029–4038.

[22] a) B.-S. Yun, J.-H. Kim, S.-Y. Kim, H.-J. Son, D. W. Cho, S. O. Kang, *Phys. Chem. Chem. Phys.* **2019**, *21*, 7155–7164; b) J. Jin, Z. Zhu, J. Yan, X. Zhou, C. Cao, P.-T. Chou, Y.-X. Zhang, Z. Zheng, C.-S. Lee, Y. Chi, *Adv. Photon. Res.* **2022**, *3*, 2100381; c) Y. Qin, X. Yang, J. Jin, D. Li, X. Zhou, Z. Zheng, Y. Sun, W.-Y. Wong, Y. Chi, S.-J. Su, *Adv. Opt. Mater.* **2022**, *10*, 2201633.

[23] a) G. Scalmani, M. J. Frisch, B. Mennucci, J. Tomasi, R. Cammi, V. Barone, *J. Chem. Phys.* **2006**, *124*, 094107; b) C. Adamo, D. Jacquemin, *Chem. Soc. Rev.* **2013**, *42*, 845–856; c) A. D. Laurent, C. Adamo, D. Jacquemin, *Phys. Chem.*

© 2025 The Author(s). Angewandte Chemie International Edition published by Wiley-VCH GmbH

15213773, 2025, 11, Downloaded from https://onlinelibrary.wiley.com/doi/10.1002/anie.202421664 by City University Of Hong Kong, Wiley Online Library on [17/03/2025]. See the Terms and Conditions (https://onlinelibrary.wiley.com/terms-and-conditions) on Wiley Online Library for rules of use; OA articles are governed by the applicable Creative Commons License

Chem. Phys. **2014**, *16*, 14334–14356; d) R. L. Martin, *J. Chem. Phys.* **2003**, *118*, 4775–4777.
[24] T. Lu, F. Chen, *J. Comput. Chem.* **2012**, *33*, 580–592.
[25] a) H. Kaji, H. Suzuki, T. Fukushima, K. Shizu, K. Suzuki, S. Kubo, T. Komino, H. Oiwa, F. Suzuki, A. Wakamiya, Y. Murata, C. Adachi, *Nat. Commun.* **2015**, *6*, 8476; b) H.-J. Cheon, S.-J. Woo, S.-H. Baek, J.-H. Lee, Y.-H. Kim, *Adv. Mater.* **2022**, *34*, 2207416; c) J. Han, Z. Huang, J. Miao, Y. Qiu, Z. Xie, C. Yang, *Chem. Sci.* **2022**, *13*, 3402–3408; d) J. Yan, Z.-Q. Feng, Y. Wu, D.-Y. Zhou, S.-M. Yiu, C.-Y. Chan, Y. Pan, K. C. Lau, L.-S. Liao, Y. Chi, *Adv. Mater.* **2024**, *36*, 2305273.
[26] X. Wang, L. Wang, G. Meng, X. Zeng, D. Zhang, L. Duan, *Sci. Adv.* **2023**, *9*, eadh1434.
[27] a) D. Hall, K. Stavrou, E. Duda, A. Danos, S. Bagnich, S. Warriner, A. M. Z. Slawin, D. Beljonne, A. Köhler, A. Monkman, Y. Olivier, E. Zysman-Colman, *Mater. Horiz.* **2022**, *9*, 1068–1080; b) X. Wu, X. Peng, L. Chen, B. Z. Tang, Z. Zhao, *ACS Materials Lett.* **2023**, *5*, 664–672; c) Z. Chen, Q. Gu, M. Li, W. Qiu, Y. Jiao, X. Peng, W. Xie, D. Liu, K. Liu, Z. Yang, S.-J. Su, *Adv. Opt. Mater.* **2024**, *12*, 2302503; d) Y.-T. Lee, C.-Y. Chan, N. Matsuno, S. Uemura, S. Oda, M. Kondo, R. W. Weerasinghe, Y. Hu, G. N. I. Lestanto, Y. Tsuchiya, Y. Li, T. Hatakeyama, C. Adachi, *Nat. Commun.* **2024**, *15*, 3174; e) T. Huang, Q. Wang, H. Zhang, Y. Xin, Y. Zhang, X. Chen, D. Zhang, L. Duan, *Nat. Mater.* **2024**, *23*, 1523–1530.
[28] a) D. S. M. Ravinson, M. E. Thompson, *Mater. Horiz.* **2020**, *7*, 1210–1217; b) A. Monkman, *ACS Appl. Mater. Interfaces* **2022**, *14*, 20463–20467; c) J. Yan, Y. Xin, Y. Pan, G. Ni, S.-M. Yiu, Y. Chi, L. Duan, K. C. Lau, *Synth. Met.* **2024**, *308*, 117734.
[29] a) S. Y. Byeon, D. R. Lee, K. S. Yook, J. Y. Lee, *Adv. Mater.* **2019**, *31*, 1803714; b) N. Haase, A. Danos, C. Pflumm, P. Stachelek, W. Brütting, A. P. Monkman, *Mater. Horiz.* **2021**, *8*, 1805–1815.
[30] Y. Gawale, R. Ansari, K. R. Naveen, J. H. Kwon, *Front. Chem.* **2023**, *11*, 1211345.
[31] a) C.-Y. Chan, M. Tanaka, Y.-T. Lee, Y.-W. Wong, H. Nakanotani, T. Hatakeyama, C. Adachi, *Nat. Photonics* **2021**, *15*, 203–207; b) H. Lee, R. Braveenth, S. Muruganantham, C. Y. Jeon, H. S. Lee, J. H. Kwon, *Nat. Commun.* **2023**, *14*, 419.
[32] a) J. Yan, Y. Wu, I.-C. Peng, Y. Pan, S.-M. Yiu, K.-T. Wong, W.-Y. Hung, Y. Chi, K.-C. Lau, *J. Mater. Chem. C* **2023**, *11*, 12270–12279; b) K. J. Kim, H. Lee, S. Kang, T. Kim, *Chem. Eng. J.* **2022**, *448*, 137671; c) C. Wu, K.-N. Tong, K. Shi, Z. Jin, Y. Wu, Y. Mu, Y. Huo, M.-C. Tang, C. Yang, H. Meng, F. Kang, G. Wei, *Adv. Sci.* **2023**, *10*, 2301112; d) Z. Zheng, L. Wang, Y. Xin, Q. Wang, X. Hong, Y. Zhang, S.-M. Yiu, F. Zhou, J. Yan, D. Zhang, L. Duan, Y. Chi, *Adv. Funct. Mater.* **2025**, *35*, 2311692.
[33] Y. Kondo, K. Yoshiura, S. Kitera, H. Nishi, S. Oda, H. Gotoh, Y. Sasada, M. Yanai, T. Hatakeyama, *Nat. Photonics* **2019**, *13*, 678–682.
[34] M. Mamada, M. Hayakawa, J. Ochi, T. Hatakeyama, *Chem. Soc. Rev.* **2024**, *53*, 1624–1692.
[35] S. Diesing, L. Zhang, E. Zysman-Colman, I. D. W. Samuel, *Nature* **2024**, *627*, 747–753.
[36] J. Zhu, M. Huang, Y. Zhang, Z. Chen, Y. Deng, H. Zhang, X. Wang, C. Yang, *Angew. Chem. Int. Ed.* **2025**, *64*, e202418770.

Manuscript received: November 7, 2024
Accepted manuscript online: January 21, 2025
Version of record online: January 28, 2025

© 2025 The Author(s). Angewandte Chemie International Edition published by Wiley-VCH GmbH

15213773, 2025, 11, Downloaded from https://onlinelibrary.wiley.com/doi/10.1002/anie.202421664 by City University Of Hong Kong, Wiley Online Library on [17/03/2025]. See the Terms and Conditions (https://onlinelibrary.wiley.com/terms-and-conditions) on Wiley Online Library for rules of use; OA articles are governed by the applicable Creative Commons License